Stem Cells Translational Medicine, 2022, **11**, 987–1001
https://doi.org/10.1093/stcltm/szac049
Advance access publication 18 August 2022
Original Research

METTL14 Regulates Osteogenesis of Bone Marrow Mesenchymal Stem Cells via Inducing Autophagy Through m^{6}A/IGF2BPs/Beclin-1 Signal Axis

Mingyu He[1,‡], Hong Lei[1,‡], Xiaoqi He[1,‡], Ying Liu[1], Ao Wang[2,3], Zijing Ren[1], Xiaoyan Liu[4], Gege Yan[1], Wenbo Wang[4], Yang Wang[2,3], Guanghui Li[1], Tong Wang[1], Jiaying Pu[2,3], Zhihua Shen[2,3], Yanquan Wang[1], Jiajie Xie[2,3], Weijie Du[1,5], Ye Yuan[2,3,5,*], Lei Yang[4,6,7,*]

[1]Department of Pharmacology, College of Pharmacy, Harbin Medical University, Harbin, People's Republic of China
[2]Department of Pharmacy (The University Key Laboratory of Drug Research, Heilongjiang Province), The Second Affiliated Hospital of Harbin Medical University, Harbin, People's Republic of China
[3]Department of Clinical Pharmacology, College of Pharmacy, Harbin Medical University, Harbin, People's Republic of China
[4]Department of Orthopedics, The First Affiliated Hospital of Harbin Medical University, Harbin, People's Republic of China
[5]Research Unit of Noninfectious Chronic Diseases in Frigid Zone, Chinese Academy of Medical Sciences, Harbin, People's Republic of China
[6]Key Laboratory of Hepatosplenic Surgery of Ministry of Education, The First Affiliated Hospital of Harbin Medical University, Harbin, People's Republic of China
[7]NHC Key Laboratory of Cell Transplantation, The First Affiliated Hospital of Harbin Medical University, Harbin, People's Republic of China

*Corresponding authors: Lei Yang, Department of Orthopedics, The First Affiliated Hospital of Harbin Medical University, Harbin 150001, People's Republic of China. Email: yangray83@vip.qq.com; Ye Yuan, Department of Pharmacy (The University Key Laboratory of Drug Research, Heilongjiang Province), The Second Affiliated Hospital of Harbin Medical University, Harbin 150001, People's Republic of China. Email: yuanye_hmu@126.com
‡M.H., H.L., and X.H. contributed equally to this work.

Abstract

The development of osteoporosis is often accompanied by autophagy disturbance, which also causes new osteoblast defects from bone marrow mesenchymal stem cells (BMSCs). However, the underlying molecular mechanisms are still not fully understood. Methyltransferase-like 14 (METTL14) is the main enzyme for N^6-methyladenosine (m^{6}A), the most prevalent internal modification in mammalian mRNAs, and it has been implicated in many bioprocesses. Herein, we demonstrate that METTL14 plays a critical role in autophagy induction and hinders osteoporosis process whose expression is decreased both in human osteoporosis bone tissue and ovariectomy (OVX) mice. In vivo, METTL14$^{+/-}$ knockdown mice exhibit elevated bone loss and impaired autophagy similar to the OVX mice, while overexpression of METTL14 significantly promotes bone formation and inhibits the progression of osteoporosis caused by OVX surgery. In vitro, METTL14 overexpression significantly enhances the osteogenic differentiation ability of BMSCs through regulating the expression of beclin-1 depending on m^{6}A modification and inducing autophagy; the opposite is true with METTL14 silencing. Subsequently, m^{6}A-binding proteins IGF2BP1/2/3 recognize m^{6}A-methylated beclin-1 mRNA and promote its translation via mediating RNA stabilization. Furthermore, METTL14 negatively regulates osteoclast differentiation. Collectively, our study reveals the METTL14/IGF2BPs/beclin-1 signal axis in BMSCs osteogenic differentiation and highlights the critical roles of METTL14-mediated m^{6}A modification in osteoporosis.

Key words: m^{6}A RNA methylation; bone marrow mesenchymal stem cells; METTL14; autophagy; osteogenic differentiation.

Received: 4 January 2022; Accepted: 5 June 2022.

Graphical Abstract

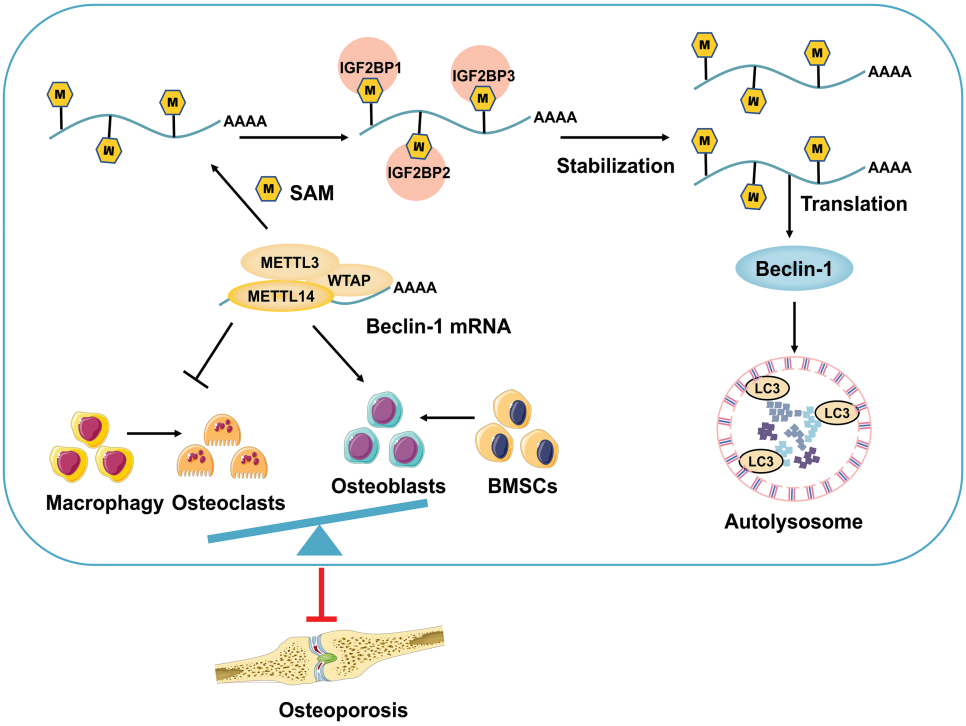

METTL14 inhibits osteoporosis development via regulating the dynamic balance between osteoblasts and osteoclasts. m6A modification of beclin-1 mediated by METTL14/IGF2BPs promotes its RNA stability and translation, which further activates autophagy and promotes osteogenic differentiation of BMSCs.

Significance Statement

The challenge of anti-osteoporosis treatments development is controlling the balance between osteoblast and osteoclast generation. This study demonstrates that METTL14 inhibits osteoporosis progression via promoting osteogenic differentiation of BMSCs and decreasing osteoclast differentiation of macrophages. We further reveal the autophagy-regulating role of METTL14 is highly potent to stimulate bone formation both in vitro and in vivo via m^{6}A/beclin-1/IGF2BPs signaling axis. Our findings provide strong evidence for the establishment of the molecular signal network regulated by m^{6}A-mediated autophagy in the occurrence and development of osteoporosis, which can serve as promising pathological predictors and therapeutic targets for patients with osteoporosis.

Introduction

Autophagy is a highly conserved catabolic activity for maintaining eukaryotic cellular homeostasis by degrading redundant organelles and macromolecules.[1,2] Increasing studies have shown that autophagy-related pathways have a crucial effect on bone homeostasis mainly including osteoclast differentiation and bone resorption.[3] Osteoporosis is characteristic of lower bone mineral density (BMD), inordinate microarchitecture, and increased risk of fragility fractures. Meanwhile, osteoporosis is associated with the imbalanced differentiation of bone marrow mesenchymal stem cells (BMSCs) containing enhanced adipogenic differentiation and weakened osteogenic differentiation.[4] Previous studies have demonstrated that autophagy decreased in both osteoporotic BMSCs and bone marrow.[5] Furthermore, autophagy is required to maintain the osteogenic differentiation of BMSCs. The autophagy inducer rapamycin could significantly promote the osteogenic differentiation of BMSCs in vitro and inhibit the process of osteoporosis in vivo.[5] Similarly, knockdown of autophagy-related genes, such as beclin-1 and ATG7 could cause a decline in autophagy following with an effective loss of bone mass in mice.[6,7] However, the specific molecular mechanism of autophagy-related genes involved in osteogenic differentiation needs to be further determined.

Previous studies have suggested that a suite of kinases responsive to various factors are involved in autophagy production, including metabolic stress, endoplasmic reticulum stress, hypoxia, and DNA damage.[8,9] It is worth noting that several studies have emphasized the great contribution of chemical modifications on RNA to autophagy signaling pathway. N^6-methyladenosine (m^{6}A) is the most prevalent post-transcriptional RNA modification in eukaryotic cells which is installed by the methyltransferase complex consisting of methyltransferase-like 3 (METTL3), methyltransferase-like 14 (METTL14), and Wilms' tumor 1-associated protein (WTAP) and deleted by demethylases, including AlkB homolog 5 (ALKBH5) and fat mass and obesity-associated protein (FTO).[10-13] Accumulating evidence has shown that m^{6}A-related enzymes participate in multiple physiological and pathological processes, such as tumor progression,[14] immune regulation,[15] stem cell differentiation[16] based on dynamically regulating the m^{6}A modification level of targeted genes. Moreover, an existing study has suggested that m^{6}A-SNPs which are associated with BMD may play important roles in the pathology of osteoporosis.[17] Recently, several

studies have found that m^{6}A modification participates the autophagy activation by modifying autophagy-related genes and further regulates a variety of physiological and pathological processes. He et al. have revealed that METTL3 could inhibit the apoptosis and autophagy of chondrocytes in inflammation via targeting m6A/YTHDF1/Bcl2 signal axis.[18] However, m^{6}A-autophagy regulation in osteoporosis is still in its infancy.

Our previous studies have demonstrated that METTL3 could promote BMSCs osteogenesis and inhibit osteoporosis development by affecting m^{6}A methylation of precursor miR-320 and RUNX2.[19] Interestingly, RNA expression of METTL14, another important m^{6}A methyltransferase, was also found to be significantly downregulated in both human and mouse osteoporotic bone tissues.[19] Thus, to further develop the molecular network of m^{6}A regulating the progression of osteoporosis, we aim to explore the regulatory effect of METTL14 on osteoporosis and whether it is possible to target autophagy.

Herein, our studies demonstrated that METTL14 is required for osteogenic differentiation of BMSCs and negatively regulates osteoclast differentiation of macrophages, so as to hold back the development of osteoporosis. Mechanistically, METTL14 promotes the m^{6}A methylation modification of beclin-1 transcripts, which can be further recognized by IGF2BPs (insulin-like growth factor 2 mRNA-binding proteins) to enhance beclin-1 expression. Accumulation of beclin-1 induces autophagy production that is beneficial to osteogenesis. Our findings provide a rationale for METTL14 being the diagnostic marker and therapeutic target to combat osteoporosis.

Methods

Human Bone Samples

Bone samples were obtained from the Department of Orthopedics, The First Affiliated Hospital of Harbin Medical University. Normal healthy bone tissues derived from the patients younger than 40 years who are involved in an accidental external trauma had surgery, whereas osteoporosis bone tissues derived from the patients older than 65 years who have severe bone loose disease had surgery. The experiments were performed under the guidance of the Experimental Animal Ethics Committee of the Harbin Medical University.

The Care and Maintenance of METTL14 Heterozygous (METTL14$^{+/-}$) Mice

METTL14 gene (NCBI reference sequence: NM_201638; Ensemb1: ENSMUSG00000028114) is located on mouse chromosome 3 and the tag termination codon is located on exon 11 (transcript: ENSMUST00000029759). Exons 7~10 were selected as the target loci. Cas9 and gRNA will be injected together into the fertilized egg to produce knockdown mice. The pups will be genotyped by PCR and then sequenced for analysis. They were cultured as F0 generation. METTL14$^{+/-}$ mice (C57BL/6J background) were purchased from Cyagen (Guangzhou, Guangdong Province, China). The animals were raised under aseptic conditions in the animal facilities of Harbin Medical University, and the animal experiment program was approved by the Institutional Animal Care and Use Committee of Harbin Medical University.

Mouse Osteoporosis Model

These assays were performed as previously described with some modifications.[19] Briefly, 8-week-old female C57BL/6 mice were selected for ovariectomy (OVX) and surgically removed both ovaries after anesthesia. They were randomly divided into Sham operation control group (exposing both ovaries and removing adjacent adipose tissue) and ovariectomized group (removing both ovaries). Experiments were performed under the Guidelines of the Institutional Animal Care and Use Committee of the Harbin Medical University.

Cell Culturing

BMSCs (C57BL/6 mice [MUBMX-01001]) were purchased from Cyagen, cultured with BMSC complete medium (MUBMX-90011; Cyagen), and incubated in an environment of 5% CO_2 at 37°C. All BMSC cells are used less than 10 passages. RAW264.7 cells were purchased from FuHeng (Shanghai, China), cultured with Dulbecco's modified Eagle's medium (DMEM) supplemented with 10% fetal bovine serum and 1% antibiotics, and incubated in an environment of 5% CO_2 at 37°C. For osteoclast differentiation induction, RAW264.7 cells were treated with 50 ng/mL RANKL (PeproTech, 315-11C, USA) in α-MEM for 5 days.

H&E Staining Assays

After the mouse was euthanized, the femur was taken, and the surrounding muscle tissue was excised. Then the tissue was fixed with 4% paraformaldehyde (PFA) (m/v) for 24 hours, fixed with 10% EDTA for 20 days, embedded in 4 μm paraffin sections, treated with H&E (hematoxylin and eosin) staining kit (Solarbio, Cat. # G1120), and observed under a fluorescence microscope. All photographs were taken under a fluorescence microscope (Leica Microsystems CMS GmbH Ernst-Leitz-Str. 17-37 D-35578 Wetzlar).

Immunochemistry Assays

The immunohistochemical (IHC) evaluation is based on the cytoplasmic reactivity and the percentage and strength of the membrane. First, the decalcification of bone tissue with 10% EDTA for 28 days and treatment with graded ethanol after paraffin sections were performed. Subsequently, antigen retrieval and primary antibody incubation were performed overnight. The next day, secondary antibody incubation was carried out for 20 minutes followed by DAB and H&E staining. Finally, gradient dehydration was performed and the slides were mounted by neutral balsam (Solarbio. cat#G8590). The primary antibodies of rabbit anti-METTL14 antibody (1:1000; Cat. # ab98166; Abcam) and rabbit anti-Beclin-1 antibody (1:1000: Cat. # P11457; Cell Signaling Technology) were used for IHC staining. All photographs were taken under a fluorescence microscope (Leica Microsystems CMS GmbH Ernst-Leitz-Str. 17-37 D-35578 Wetzlar).

TRAP Staining

The obtained mouse femurs were decalcified in EDTA decalcification solution for at least 28 days, followed by dehydration, and then embedded in 4 μm paraffin sections. The sections were dewaxed, stained with tartrate-resistant acid phosphatase (TRAP) dye at 37°C for 3 hours, soaked in distilled water at 37°C for 3 minutes, counterstained with methyl green for 2~3 minutes, and then dehydrated and sealed. All photographs were taken under a fluorescence

microscope (Leica Microsystems CMS GmbH Ernst-Leitz-Str. 17-37 D-35578 Wetzlar).

Quantitative Real-Time Polymerase Chain Reaction

Total RNA was extracted from bone tissues and BMSCs using TRIzol reagent. The synthesis of cDNA was performed using the High Capacity cDNA Reverse Transcription Kit (Cat. # 00676299; Thermo Fisher Scientific, Waltham, MA, USA) according to the manufacturer's instructions. Amplification and detection were performed using a 7500-HT Fast Real-Time PCR system (Applied Biosystems, Waltham, MA, USA) with SYBR Green PCR Master Mix (Cat. # 31598800; Roche). The measured expression level of each gene was normalized to that of glyceraldehyde-3-phosphate dehydrogenase (GAPDH). Supplementary Table S1 lists the sequence information for the primers used in this study.

Adenovirus Injection

Adenovirus particles containing pAV[Exp]-CMV>METTL14 vector or pAV[Exp]-CMV>empty vector were obtained from Cyagen. Twenty-four female 8-week-old C57BL/6 mice were randomly divided into two groups to receive adenovirus treatment. METTL14-carrying adenovirus of 20 μL (titer: 1×10^{10} PFU/mL) or empty vector adenovirus of an equal volume was intramuscularly vertically injected into the lateral thigh muscle of the mice every 2 days for three consecutive injections. Then each group was again randomly divided into two groups for OVX or Sham surgery.

Micro-CT Analysis

The femurs of model mice were fixed in 4% paraformaldehyde (PFA) at 4°C for 48h and decalcified with 10% EDTA for 3 weeks . Next, Skyscan1076 instrument (SkyScan, Belgium) was used to analyze the gross bone morphology and microstructure. Then BV/TV, Tb.Th, Tb.N, and Tb.Sp were analyzed.

Plasmid and siRNA Transfection

BMSCs were seeded in a 6-well plate at a concentration of 2×10^5 cells per 2 mL in the medium. METTL14-carrying or beclin-1-carrying plasmids or negative control plasmids were transfected with Lipofectamine 3000 Reagent (MAN0009872; Invitrogen, Carlsbad, CA, USA) according to the manufacturer's instructions. siRNA or a negative control oligonucleotide was transfected into BMSCs with Lipofectamine RNAiMAX Reagent (MAN0007825; Invitrogen) according to the manufacturer's instructions. After 24 hours, subsequent experimental measurements were performed. The sequences of siRNAs used are METTL14: sense 5′-GCAGCACCUCGGUCAUUUATT-3′ and antisense 5′-UAAAUGACCGAGGUGCUGCTT-3′; IGF2BP1 siRNA: sense 5′-UUUACUUCCUCCUUGGGACUU′ and antisense 5′-GUCCCAAGGAGGAAGUAAATT-3′; IGF2BP2 siRNA: sense 5′-ACACAUCAAACAGCUCGCUCGAUUU-3′ and antisense 5′-AAAUCGAGCGAGCUGUUUGAUGUGU-3′ and IGF2BP3 siRNA: sense 5′-AAAUGAUAUUGCUUCCAUGAAUCTT-3′ and antisense 5′-GAUUCAUGGAAGCAAUAUCAUUUTT-3′.

Induction of Osteogenic Differentiation

BMSCs were seeded in a 6-well plate coated with gelatin (GLT-11301; Cyagen) at the density of 2×10^4 cells/cm^2. 2 mL osteogenic differentiation medium (MUBMX-90021; Cyagen) was carefully added to the plate, when the cell confluence reached 60%-70%. The fresh induction medium was replaced every 3 days.

ARS Staining

Cells were fixed for 15 minutes with 4% formaldehyde at 37°C, washed with phosphate-buffered saline (PBS) three times, and then stained with 40 mM ARS (alizarin red staining) solution (S0141; Cyagen) for 5 minutes. Finally, the ARS solution was removed, washed with PBS, and observed using light microscopy (Eclipse TS100; Nikon, Melville, NY, USA). The results were calculated using ImageJ software (National Institutes of Health [NIH], USA).

ALP Staining Assay

Cells were fixed with 4% formaldehyde at 37°C for 15 minutes and then washed with deionized water three times, mixed with fast red violet (FRV) alkaline solution (22.2 μL) and sodium nitrite solution (22.2 μL) at room temperature (RT) for 2 minutes, and then mixed with 1 mL deionized water containing 22.2 μL AS-BI alkaline solution. Then cells were covered with the mixed solution in the dark for 15 minutes at RT. Then cells were rinsed with deionized water for 2 minutes and covered with hematoxylin solution for 5 minutes and finally rinsed with deionized water two times. Images were observed using standard light microscopy (Eclipse TS100; Nikon).

Western Blot Analysis

Cells with different treatments or bone tissues were harvested for Western blot analysis and lysed with 50 μL of RIPA (radioimmunoprecipitation assay) buffer. After three times of ultrasound, the protein supernatant was extracted by centrifugation at 12 000 g for 15 minutes, and the protein concentration was determined by the BCA kit. The loading quantity of protein sample is 30 μg, and the loading volume is 20 μL. After completion, SDS-PAGE electrophoresis was performed and transferred to the nitrocellulose filter membrane. Then it was blocked with 5% non-fat dry milk in a shaker for 1 hour and then incubated with primary and secondary antibodies. Primary antibodies against P62 (5114), ATG5 (12994), ATG3 (3415), ATG7 (8558), ATG12 (4180), beclin-1 (3495), RUNX2 (12556) were purchased from Cell Signaling Technology. Antibody specific for LC3 (L7643) was purchased from Sigma-Aldrich. Antibodies specific for GAPDH (AC002), OCN (A1530), and β-tubulin (AC021) were purchased from ABclonal. Antibody specific for METTL14 (ab98166) was purchased from Abcam. Antibody specific for ALP (alkaline phosphatase, sc-365765) was purchased from Santa Cruz Biotechnology. Secondary antibodies were anti-mouse IgG (ImmunoWay Biotechnology, RS23910) or anti-rabbit IgG (ImmunoWay Biotechnology, RS23920). Western blot bands were imaged with Odyssey CLX and quantified with LI-COR Image Studio Software.

RNA-binding Protein Immunoprecipitation qPCR

RNA-binding protein immunoprecipitation qPCR (RIP-qPCR) was performed using Magna MeRIP Kit (Millipore, Cat. # CR203146) according to the manufacturer's instruction. Briefly, cells were harvested with ice-cold PBS and centrifuged at 4°C at 1000 g for 5 minutes and then the supernatant was discarded, and 100 μL RIP lysis buffer was added and incubated on the ice at −80°C for 5-minutes. Then,

antibody (5 μg) and magnetic beads were added to the test tube and spun to mix for 30 minutes at RT and washed the magnetic beads twice with RIP wash buffer. Then the cells were resuspended in RIP buffer (900 μL) and cell lysate (100 μL), which is then centrifuged at 4°C at 14 000 g for 10 minutes. The mixture was rotated overnight at 4°C and washed with high salt buffer. Finally, RNA was extracted with RIP wash buffer and analyzed by quantitative real-time polymerase chain reaction (qRT-PCR).

Calcein Double-Labeling Experiment

Mice were killed after intraperitoneally injected with calcein (10 μg/g, PBS configuration) 2 day and 8 day. The femurs and tibias on both sides were dissected and placed in 4% PFA at 4°C for 48 hours and stored in the dark. Frozen sections were performed on the femurs at 4 μm, and the sections were stored away from light. After observation under a confocal microscope, images were collected and quantitatively analyzed with LAS V4.13 software.

RNA Half-Life Detection

Actinomycin D (Act D, 5 μg/mL) was added to the cells, and RNA was extracted after incubation for 0, 3, and 6 hours. qRT-PCR was used to detect the half-life of mRNA.

Protein Half-Life Detection

The cells were treated with 100 mg/mL cycloheximide (CHX), and the cells were collected at the time points of 0 and 8 hours according to the instructions, and the protein was extracted. Afterwards, Western bolt experiments were performed on the extracted proteins.

Live Cell Imaging for Autophagic Flux

When autophagosomes bind to lysosomes, the green fluorescent protein (GFP) fluorescence will be quenched, but red fluorescence can be observed. The cells were infected with mRFP-GFP-LC3 adenoviral (HanBio, Shanghai, China) and washed with DMEM for 6 hours after transfection and continued to culture the cells for 48 hours; finally, images were observed on a confocal laser scanning microscope (FV10i).

Electron Microscopy

BMSCs were fixed by 2.5% glutaraldehyde buffer (pH 7.4) at 4°C overnight. Then 1% osmium tetroxide was used to fix the samples for 1 hour at RT. Next, the cells was dehydrated with gradient ethanol and embedded in paraffin. The samples were stained with saturated uranyl acetate and lead citrate. Finally, the cells were observed under a transmission electron microscope (Hitachi 7650, Tokyo, Japan) at 80KV.

Statistical Analysis

Data were analyzed by GraphPad Prism version 7 and expressed as mean ± SD. Statistical analysis was performed unpaired *t*-test while there was one variance between the two groups. ANOVA was applied for multiple group comparisons, while one-way ANOVA was used for one variance analysis. All experiments were independently repeated at least three times. P values <.05 were considered statistically significant, with $^{*}P < .05$; $^{**}P < .01$; $^{***}P < .001$.

Results

METTL14 Knockdown (METTL14$^{+/-}$) Mice Exhibit Elevated Bone Loss and Autophagy Defects Similar to OVX Mice

To identify the correlation between osteoporosis and autophagy, we first established the mice osteoporosis model by ovariectomized surgery. Compared to the Sham mice group, bone formation in the OVX mice group, as assessed by calcein double labeling and MAR (mineral apposition rate) quantification, was markedly declined (Fig. 1A). Further examination indicated that the expression of P62, a key protein of autophagy, was elevated in the bone tissue of OVX mice compared with that of Sham mice, along with the decrease in the protein level of the LC3II/LC3I ratio, indicating a blockage of autophagy (Fig. 1B). Our previous study has shown that the mRNA expression of m^{6}A methyltransferase METTL14 is downregulated in the development of osteoporosis.[19] To further verify this phenomenon, we examined METTL14 protein expression in bone tissue from patients with osteoporosis and OVX mice, respectively. Consistently, protein expression of METTL14 was also at a lower level both in the bone tissue of patients with osteoporosis and OVX mice than those of normal person and Sham mice (Fig. 1C). Meanwhile, IHC staining results also presented that METTL14 level was decreased in the bone of OVX mice (Fig. 1D), suggesting that the downregulation of METTL14 in the development of osteoporosis is common. As METTL14 homozygous mice have been reported to die during the embryonic period in the mother,[20] we selected METTL14 heterozygous knockdown (METTL14$^{+/-}$) mice for the next experimental study (Fig. 1E). As shown in Supplementary Fig. S1A, S1B, the METTL14 level was markedly decreased on both mRNA and protein expression levels in bone tissue in METTL14$^{+/-}$ mice. Interestingly, calcein double labeling and Western blot results showed that METTL14$^{+/-}$ mice exhibited lower MAR (Fig. 1F) along with higher protein expression of P62 and smaller ratio of LC3II/LC3I (Fig. 1G). Therefore, these results indicated that METTL14 knockdown leads to the inhibition of bone formation and the reduction of autophagosome formation similar to OVX surgery.

METTL14 Promotes Bone Formation and Inhibits Osteoporosis Development In Vivo

Next, we performed OVX in wild-type (WT) and METTL14$^{+/-}$ mice, and used micro-computed tomography (micro-CT) scans to detect bone mass and bone formation. Interestingly, after 2 months of surgery, bone mass and bone formation ability of METTL14$^{+/-}$ mice were both further decreased, compared with WT mice in both Sham and OVX groups, along with reduced bone volume per tissue volume (BV/TV), trabecular number (Tb.N) and trabecular thickness (Tb.Th) as well as increased trabecular separation (Tb.Sp) (Fig. 2A, 2B). Moreover, H&E-stained bone sections showed that fewer trabeculae had developed in METTL14$^{+/-}$ mice (Fig. 2D). Meanwhile, we used an adenoviral gene delivery system to overexpress METTL14 by multisite intramuscular injection in C57BL/6 mice and performed OVX surgery after injection 7 days. As shown in Fig. 2D, METTL14 levels were significantly increased at both mRNA and protein expression levels in bone tissue from the mice injected with METTL14 adenovirus (Ad-METTL14) compared to those of mice injected with empty adenovirus

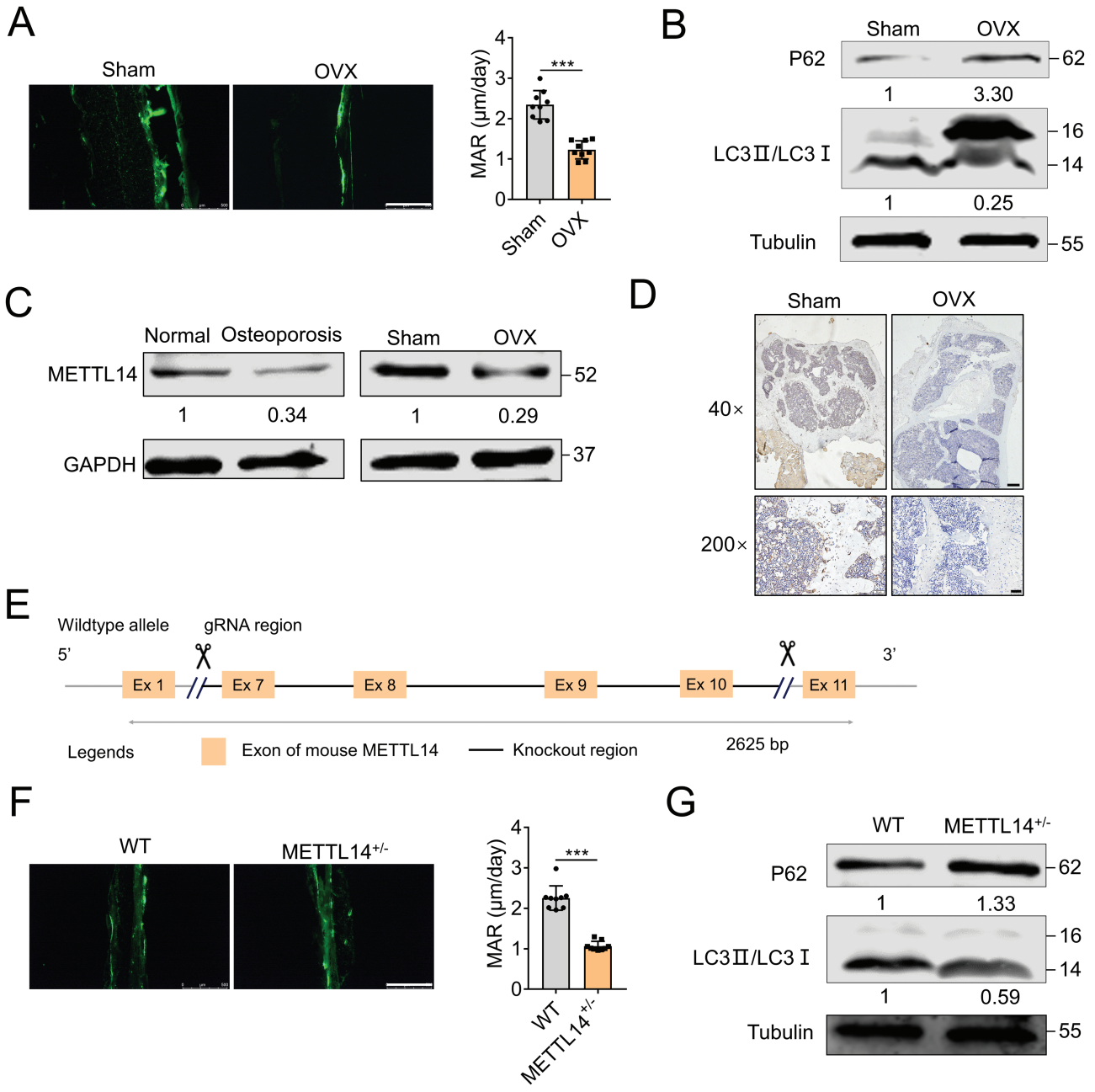

Figure 1. METTL14$^{+/-}$ mice exhibit elevated bone loss and defects of autophagy. (A) Representative images of calcein double labeling of trabecular bone of the Sham-operated (Sham) and the ovariectomized (OVX) mice with quantification of MAR. Scale bar = 100 μm. $n = 9$. (B) Western blotting of P62, LC3II/I in the bone tissue Sham and OVX mice. (C) Western blotting of METTL14 in the human bone from normal and osteoporosis (left) and in Sham and OVX mice (right). (D) Immunohistochemistry (IHC) analysis of METTL14 protein expression in the bone tissues of Sham and OVX mice. Representative IHC images (magnification ×40 and ×200) are presented (scale bar = 200 μm (upper) and 50 μm (lower), $n = 3$). (E) Schematic illustration of generation of METTL14$^{+/-}$ mice (C57BL/6) by CRISPR/Cas9-mediated genome engineering strategy. (F) Representative images of calcein double labeling of trabecular bone of WT and METTL14$^{+/-}$ mice with quantification of MAR. Scale bar = 100 μm. $n = 9$. (G) Protein expression of P62, LC3II/LC3I in the bone tissues of WT and METTL14$^{+/-}$ mice. Data are expressed as mean ± SD. ***$P < .001$.

(Ad-empty). Two months after the establishment of the osteoporosis model, we detected the efficiency of METTL14 expression, and the results showed that METTL14 protein expression was still significantly increased in Ad-METTL14 group (Supplementary Fig. S1C). According to the results of micro-CT, after OVX surgery, compared to OVX-Ad-empty group, METTL14 overexpression significantly reduced symptoms of osteoporosis caused by OVX surgery as the BV/TV, Tb.N, and Tb.Th were increased and Tb.Sp was decreased (Fig. 2E, 2F). Taken together, those results indicated that METTL14 deficiency inhibits bone formation following with the decrease of autophagy.

METTL14 Promotes the Osteogenic Differentiation Ability of BMSCs via Autophagy Activation

The main reason for exacerbating the process of osteoporosis is the imbalance shift of BMSCs from osteogenic differentiation to adipogenic differentiation.[21] Thus, we detected the change of METTL14 protein level during osteogenic differentiation of BMSCs. As shown in Fig. 3A, METTL14

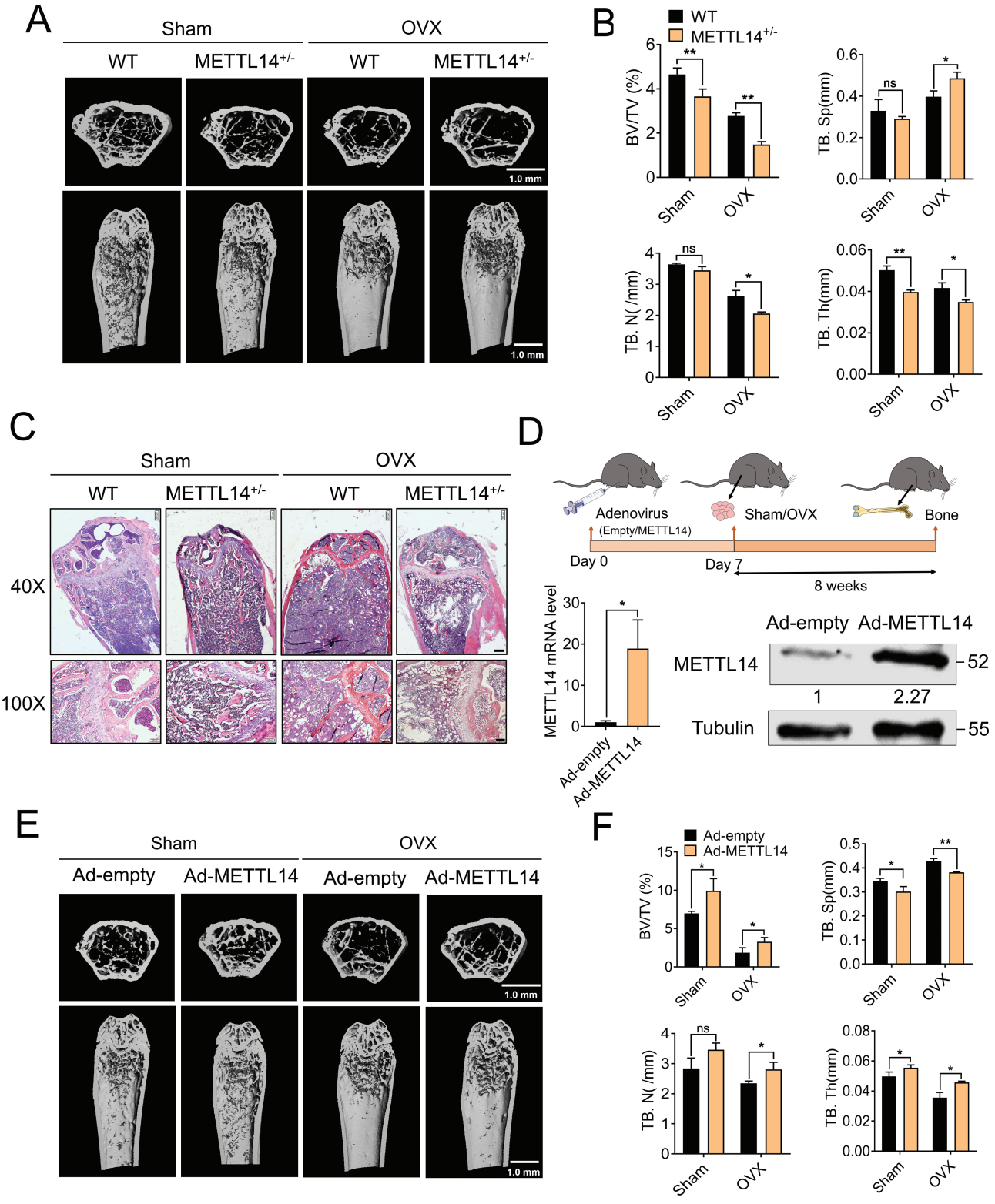

Figure 2. The negative impact of METTL14$^{+/-}$ on bone mass and density and overexpression of METTL14 rescues impaired bone microstructure and bone mass in OVX mice. (A) Micro-CT images of trabecular bone of the femoral metaphysis (upper panels) and entire proximal femur (lower panels) show the impairment of bone microstructure in METTL14$^{+/-}$ mice without OVX and the enhanced impairment of bone microstructure in METTL14$^{+/-}$ mice with OVX. Scale bar = 1.0 mm. $n = 3$. (B) Micro-CT analysis shows the decreases in bone volume/tissue volume ratio (BV/TV), trabecular number (Tb.N), and trabecular thickness (Tb.Th) and the increase in trabecular separation (Tb.Sp). $n = 3$. (C) Representative H&E staining images of WT and METTL14$^{+/-}$ mouse femurs (scale bar = 200 μm [upper] and 100 μm [lower], $n = 3$). (D) Schematic drawing of the timer shaft for mice adenovirus injection and ovariectomy surgery (top). qRT-PCR and Western blot results show the efficiency of virus infection of mice bone tissues (bottom). (E) Representative micro-CT images of trabecular bone of the femoral metaphysis (top) and entire proximal femur (bottom) show the rescuing effects of METTL14 adenovirus on the impaired bone microstructure in OVX mice. Scale bar = 1.0 mm. $n = 4$. (F) Micro-CT analysis statistical data of BV/TV, Tb.N, Tb.Sp, and Tb.Th both in femur from 4-month-old females of the Ad-empty and Ad-METTL14 mice. $n = 4$. Data are expressed as mean ± SD. $^{*}P < .05$; $^{**}P < .01$.

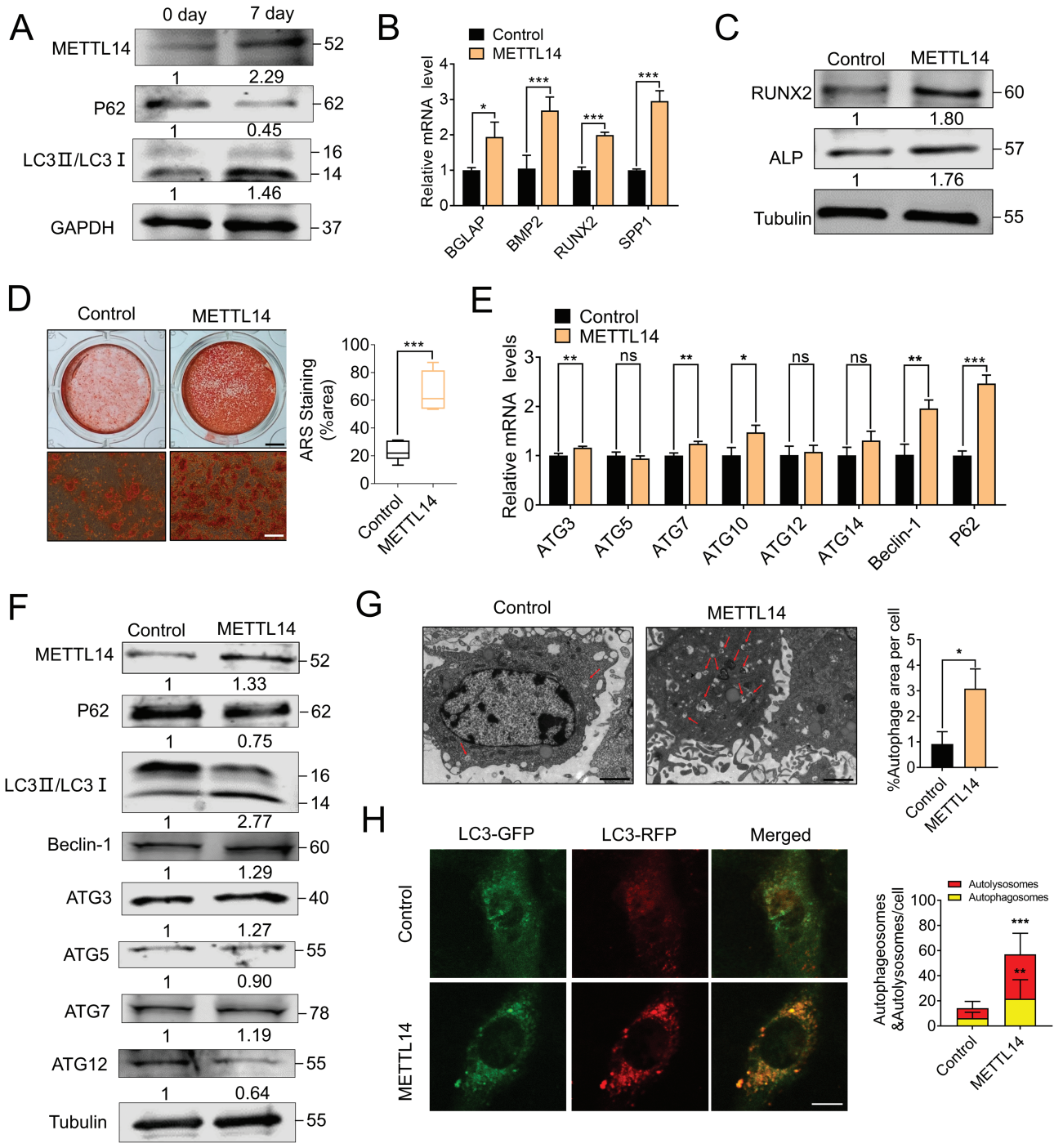

Figure 3. Overexpression of METTL14 promotes osteogenic differentiation and autophagy of BMSCs. (A) Verification of protein METTL14 level at day 0 and day 7 after osteogenesis induced in BMSCs. (B) mRNA expression levels of osteogenesis-related genes (BGLAP, BMP2, RUNX2, and SPP1) in BMSCs administration of the function of METTL14 overexpression (METTL14) or the empty vector-carrying adenovirus (Control) as determined by qRT-PCR. $n = 3$. (C) Western blotting of RUNX2 and ALP in Control and METTL14 group. $n = 3$. (D) Representative images of ARS staining (left panel) and statistical data (right panel) of BMSCs from control and METTL14. Scale bar = upper: 2 mm; lower: 200 μm. $n = 6$. (E) mRNA expression levels of autophagy-related genes (ATG3, ATG5, ATG7, ATG10, ATG12, ATG14, beclin-1, and P62) in control and METTL14, as determined by qRT-PCR. $n = 3$. (F) Western blotting of P62, LC3II/LC3I, beclin-1, ATG3, ATG5, ATG7, and ATG12 after transfected with or without METTL14 plasmids. $n = 3$. (G) Representative electron microscope images (left panel) and statistical data (right panel) show the change of autophagy production after METTL14 overexpression in BMSCs. Scale bar = 2 μm. $n = 3$. (H) Representative immunofluorescence images (left panel) and statistical data (right panel) show the localization of LC3 in autolysosomes and autophagosomes with anti-GFP and anti-RFP antibodies to verify the effect of METTL14 on autophagy. Scale bar = 10 μm. $n = 6$. Data are expressed as mean ± SD. $^*P < .05$; $^{**}P < .01$; $^{***}P < .001$.

expression was significantly increased with 7 days of osteogenic induction of BMSCs. Notably, autophagy was also increased during this process as the protein level of P62 was downregulated and the ratio of LC3II/LC3I was upregulated.

To further investigate the role of METTL14 in BMSCs differentiation, we both performed gain-of-function studies. We thus overexpressed METTL14 in BMSCs and verified the transfection efficiency of day 1 and day 7, respectively

(Supplementary Fig. S2A, S2B). In agreement with the in vivo results, the mRNA expression levels of critical osteogenesis-related genes containing bone gamma carboxy glutamate protein 2 (BGLAP), bone morphogenetic protein 2 (BMP2), runt-related transcription factor 2 (RUNX2), secreted phosphoprotein 1 (SPP1), and the protein level of RUNX2 and ALP, compared to control group, were significantly increased with METTL14 overexpression after 7 days osteogenic differentiation (Fig. 3B, 3C). Additionally, forced expression of METTL14 also markedly enhanced extracellular matrix mineralization (EMM) according to the results of ARS (Fig. 3D). To directly evaluate the effects of METTL14 on autophagy, we firstly detected the mRNA expression of autophagy-related genes with or without METTL14 overexpression. qRT-PCR (Fig. 3E) and Western blot (Fig. 3F) results showed that the mRNA levels of ATG3, ATG7, ATG10, beclin-1 and P62 and the protein levels of LC3II/LC3I ratio, beclin-1, ATG3, ATG7 were both increased and P62 protein expression was decreased when METTL14 was overexpressed, with beclin-1 being the most significantly elevated. Consistently, transmission electron microscopy (TEM) analysis showed that the area of autophagic vesicles per cell was markedly increased with METTL14 overexpression (Fig. 3G). Meanwhile, more ectopically expressed mRFP-GFP-LC3 was observed as red (autolysosome formation) and yellow (autophagosome formation) speckles in the METTL14 overexpression group cells than that in control group cells (Fig. 3H).

Oppositely, we performed loss-of-function studies through knocking down METTL14 by small interfering RNAs (siRNAs) and verified the knockdown efficiency of day 1 and day 7, respectively (Supplementary Fig. S2C, S2D). As expected, METTL14 silencing markedly suppressed the expression of osteogenesis-related genes both in mRNA and protein (Fig. 4A, 4B), as well as a reduction of osteoblastic nodules detected by ARS staining (Fig. 4C). Furthermore, qRT-PCR results showed that downregulation of METTL14 decreased mRNA expression of partial autophagy-related genes containing ATG3, ATG5, ATG12, ATG14, and beclin-1 (Fig. 4D). In agreement, the protein level of beclin-1, ATG3, ATG5, and the ratio of LC3II/LC3I was significantly decreased and p62 protein level was increased with METTL14 knockdown (Fig. 4E). According to these results, we observed that beclin-1 and ATG3 were the autophagy-related genes most strongly positively regulated by METTL14. Similarly, the number of autophagosomes and autolysosomes and the intensity of LC3 puncta were significantly reduced (Fig. 4F). Taken together, we hypothesized that the regulation of METTL14 in BMSCs osteogenic differentiation is possibly due to the autophagy induction via targeting autophagy key regulatory genes.

Beclin-1 Is Functionally Essential Target of METTL14 in Autophagy Activation During BMSCs Osteogenic Differentiation

We then conducted gene-specific m^{6}A-qPCR assays in BMSCs to identify whether beclin-1 or ATG3 was the target of METTL14. As shown in Fig. 5A, the m^{6}A abundance of beclin-1 was obviously decreased upon METTL14 knockdown, while ATG3 showed no significant change (Supplementary Fig. S3). Interestingly, according to a sequence-based m^{6}A modification site predictor, we observed that beclin-1 gene carries 7 high and moderate confidence potential m^{6}A modification sites (http://www.cuilab.cn/sramp; Fig. 5B). Notably, recent studies have revealed that beclin-1 plays a vital role in BMSCs differentiation which is significantly reduced in OVX BMSCs compared to Sham BMSCs.[5] Consistently, IHC results showed a remarkable reduction of beclin-1 protein in OVX mice bone tissues compared to those of Sham mice (Fig. 5C). Furthermore, Western blot results showed that beclin-1 protein expression was reduced in bone tissue from METTL14$^{+/-}$ mice, whereas the opposite is true with METTL14 ectopic expression in mice (Fig. 5D). It has been confirmed that m^{6}A modification on mRNA transcripts could affect mRNA stability and protein degradation. To investigate whether METTL14 regulates beclin-1 expression through modulating its mRNA stability, we treated BMSCs with the transcription inhibitor Act D and detected the half-lives of beclin-1 transcripts. Indeed, as shown in Fig. 5E, METTL14 silencing caused a noticeable decrease in the half-lives of beclin-1 transcripts (9.13-6.14 hours). In contrast, METTL14 overexpression resulted in a remarkable increase of beclin-1 transcripts (5.17-15.49 hours, Fig. 5E), suggesting that METTL14-induced upregulation of beclin-1 expression is at least in part due to the enhanced stability of beclin-1 mRNA transcripts upon METTL14-mediated increase of m^{6}A level in its mRNA transcripts. In order to determine the mechanism of the strong increase in beclin-1 protein under METTL14 overexpression and the clear decrease of beclin-1 with METTL14 silencing, we examined the stability of the protein by blocking protein synthesis using CHX. After 8 hours of CHX treatments, the beclin-1 protein degradation rate was observably accelerated by METTL14 knockdown (Supplementary Fig. S4A), whereas METTL14 forced expression put off it (Supplementary Fig. S4B).

To further verify that METTL14-mediated osteogenic differentiation partially relies on autophagy activation, we co-treated BMSCs both with METTL14 overexpression and 3-methyladenine (3-MA), an autophagy inhibitor, and then performed an osteogenesis induction. As expected, treatment with 3-MA indeed decreased the expression of key osteogenesis-related genes, including RUNX2 and BMP4 (Fig. 5F, 5G). Subsequently, as beclin-1 may be the potential target of METTL14, we overexpressed beclin-1 based on the knockdown of METTL14 to further investigate the role of beclin-1 in the osteogenesis of BMSCs regulated by METTL14. As shown in Fig. 5H, 5I, introducing the expression of beclin-1 in METTL14 knockdown cells promoted the mRNA expression of ALP, BMP4 as well as ALP protein levels, which were inhibited by METTL14 silencing. Consistently, a deceleration in the activity of ALP was observed upon 3-MA treatment detected by ALP staining (Fig. 5J), while forced expression of beclin-1 rescued the ALP activity inhibition caused by METTL14 knockdown (Fig. 5K). Collectively, autophagy maintenance ensured by METTL14 mediated beclin-1 mRNA stability and translation is essential for osteogenic differentiation of BMSCs, thereby hindering the development of osteoporosis.

The m^{6}A Reading IGF2BP Proteins Promote the mRNA Stability of Beclin-1

mRNAs that undergo m^{6}A modification to perform specific biological functions require a specific RNA-binding protein, the methylated reading protein, also known as reader. Earlier studies revealed that IGF2BPs stabilize methylated mRNAs and further enhance translation.[22] To elucidate the specific m^{6}A readers of beclin-1, and determine the m^{6}A-dependent mechanism of beclin-1 regulation, we performed RIP-qPCR

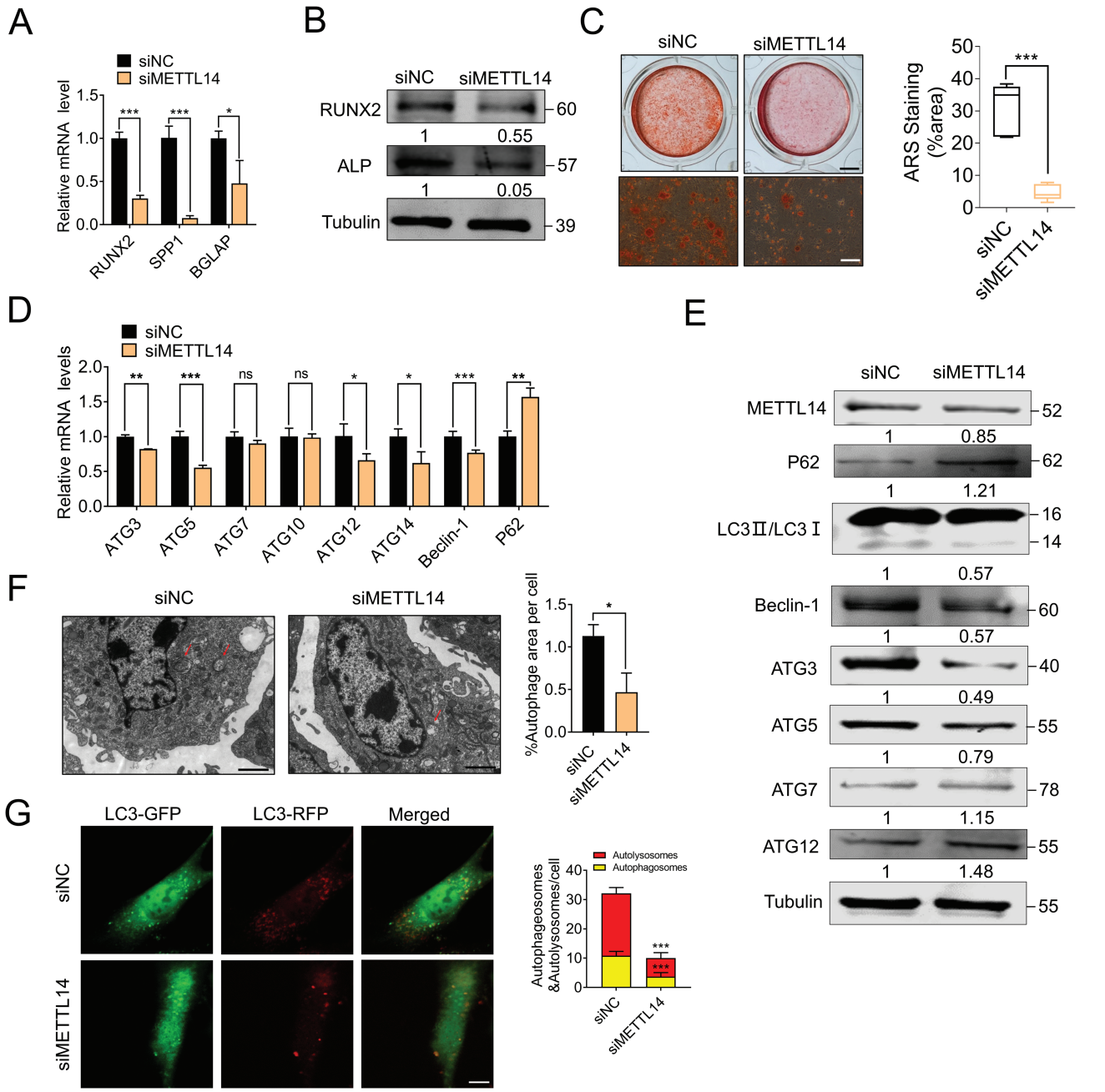

Figure 4. Silence of METTL14 blocks osteogenic differentiation and autophagy of BMSCs. (A) mRNA expression levels of osteogenesis-related genes (RUNX2, SPP1, BGLAP) in BMSCs transfection with negative control (siNC) and METTL14 siRNA (siMETTL14), as determined by qRT-PCR. $n = 3$. (B) Western blotting of RUNX2 and ALP in siNC and siMETTL14. (C) Representative images of ARS staining (left panel) and statistical data (right panel) of BMSCs from siNC and siMETTL14. Scale bar = upper: 2 mm; lower: 200 μm. $n = 6$. (D) mRNA expression levels of autophagy-related genes (ATG3, ATG5, ATG7, ATG10, ATG12, ATG14, beclin-1, and P62) in BMSCs infected with NC or METTL14 siRNA, as determined by qRT-PCR. $n = 3$. (E) Western blot results show the METTL14, P62, LC3II/LC3I, beclin-1, ATG3, ATG5, ATG7, and ATG12 protein levels in BMSCs induced by NC and METTL14 silencing. $n = 3$. (F) Representative electron microscope images (left panel) and statistical data (right panel) show the autophagy of the function of METTL14 knockdown in BMSCs. Scale bar = 2 μm. $n = 3$. (G) Representative immunofluorescence images (left panel) and statistical data (right panel) show the localization of LC3 in autolysosomes and autophagosomes with anti-GFP and anti-RFP to verify the effect of weakening METTL14 on autophagy. $n = 6$. Scale bar = 10 μm. Data are expressed as mean ± SD. $^*P < .05$; $^{**}P < .01$; $^{***}P < .001$.

assay to screen for beclin-1-related m^{6}A readers. Interestingly, the results validated that IGF2BP1, IGF2BP2, and IGF2BP3 antibodies could pull down the beclin-1 mRNA, indicating that IGF2BP1, IGF2BP2, and IGF2BP3 proteins combined with beclin-1 mRNA (Fig. 6A). Subsequently, knockdown of IGF2BP1/2/3 resulted in a marked decrease in mRNA and protein levels of beclin-1 (Fig. 6B-6E). Simultaneously their knockdown efficiency was verified by qRT-PCR (Supplementary Fig. S5A-S5C). In addition, as shown in Fig. 6F-6H, IGF2BP1/2/3 silencing reduced the stability of beclin-1 mRNA in the presence of transcription inhibitor Act D in BMSCs. Taken together, those results indicated that the methylated beclin-1 transcripts were directly recognized by the m^{6}A "reader," IGF2BP proteins, which maintained the

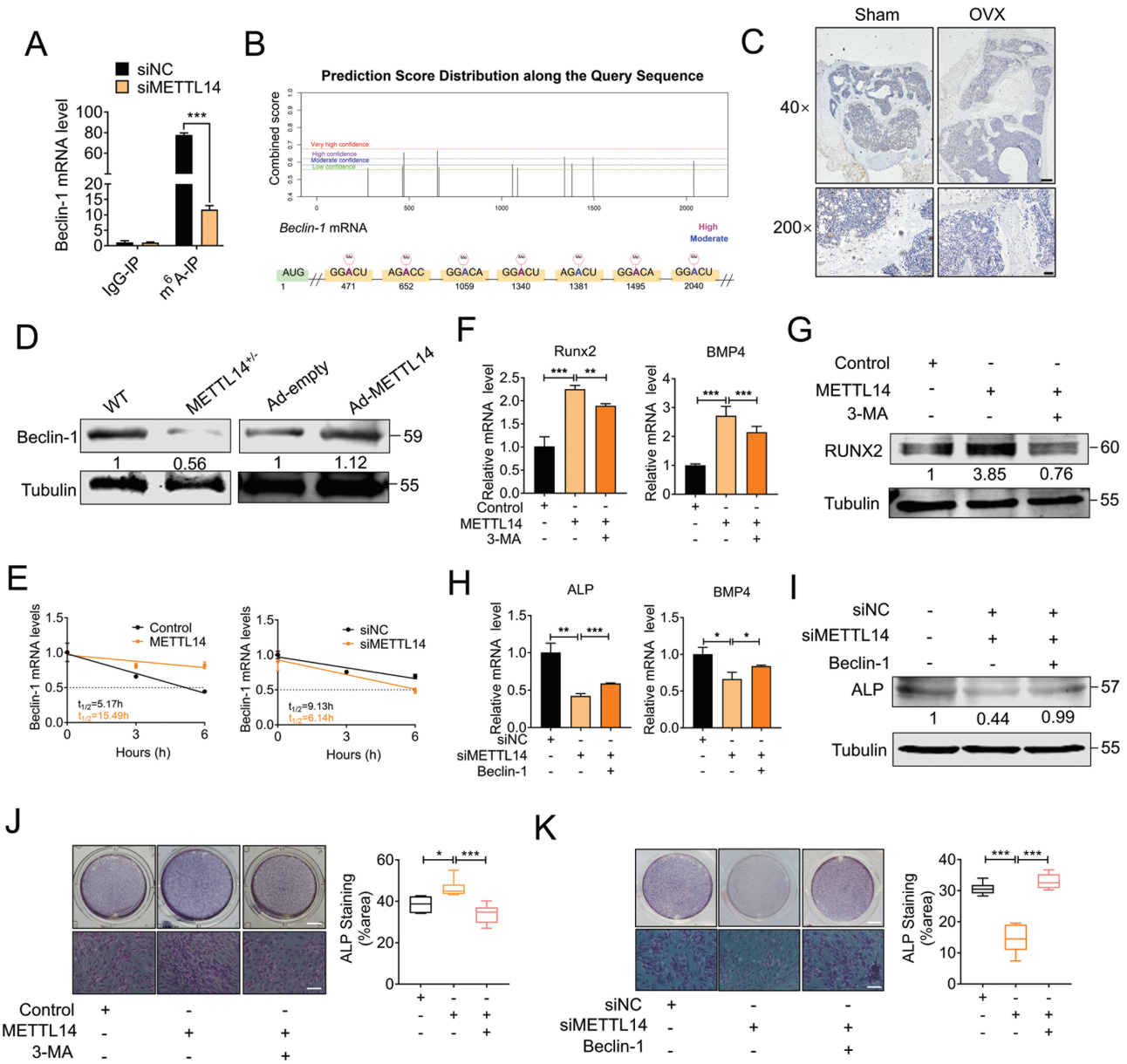

Figure 5. METTL14 regulates mRNA stability and translation of beclin-1. (A) Gene-specific m^{6}A-qPCR assay shows the reduction of m^{6}A modification in specific regions of beclin-1 gene by METTL14 silencing in BMSCs. (B) Potential sites and regions for m^{6}A modification in the sequence of beclin-1 gene. (C) Immunohistochemistry (IHC) analysis of beclin-1 protein expression in bone tissues of Sham and OVX mice. Representative IHC images (magnification ×40 and ×200) are presented (scale bar: 200 μm and 50 μm. $n = 3$). (D) Western blot results show the beclin-1 protein level in WT, METTL14$^{+/-}$, Control, and METTL14 mice, respectively. $n = 3$. (E) qRT-PCR shows beclin-1 transcripts stability in Act D-treated cells forced expression of METTL14 (left) and METTL14 silencing (right). $n = 3$. (F) mRNA expression levels of osteogenesis-related genes (RUNX2, BMP4) in BMSCs after being transfected with METTL14 plasmids and/or co-transfected with beclin-1 inhibitor (3-MA), as determined by qRT-PCR. $n = 3$. (G) Western blot results show the RUNX2 protein level after transfected with METTL14 plasmids with or without the presence of 3-MA. $n = 3$. (H) mRNA expression levels of osteogenesis-related genes (ALP, BMP4) in BMSCs by the function of METTL14 knockdown with or without beclin-1, as determined by qRT-PCR. $n = 3$. (I) Western blot results show the ALP protein level in METTL14 silence with or without forced expression of beclin-1. $n = 3$. (J) Representative images of ALP staining (left panel) and statistical data (right panel) of BMSCs show the effects of METTL14 overexpression with or without 3-MA treatment on the osteogenic ability. $n = 6$. (K) Counteracting effect of beclin-1 to the weakening of osteogenic ability after METTL14 silencing, as indicated by ALP staining. $n = 6$. Data are expressed as mean ± SD. *$P < .05$; **$P < .01$; ***$P < .001$.

stability of the transcripts to prevent its degradation and naturally increase its expression via an m^{6}A-IGF2BPs-dependent mechanism.

METTL14 Negatively Regulates Osteoclast Differentiation

The hyperactivity of osteoclasts leads to increased bone resorption, which is further decomposed and absorbed by acids and enzymes secreted by osteoclasts, contributing to overall bone mass downregulation and leading to osteoporosis.[23] In order to comprehensively clarify the role of METTL14 in the treatment of osteoporosis, we further investigated the role of METTL14 in osteoclast differentiation. To further verify the regulatory effect of METTL14 on osteoclast differentiation in vivo, we performed TRAP-specific staining to detect the osteoclast numbers of the mouse femur. As

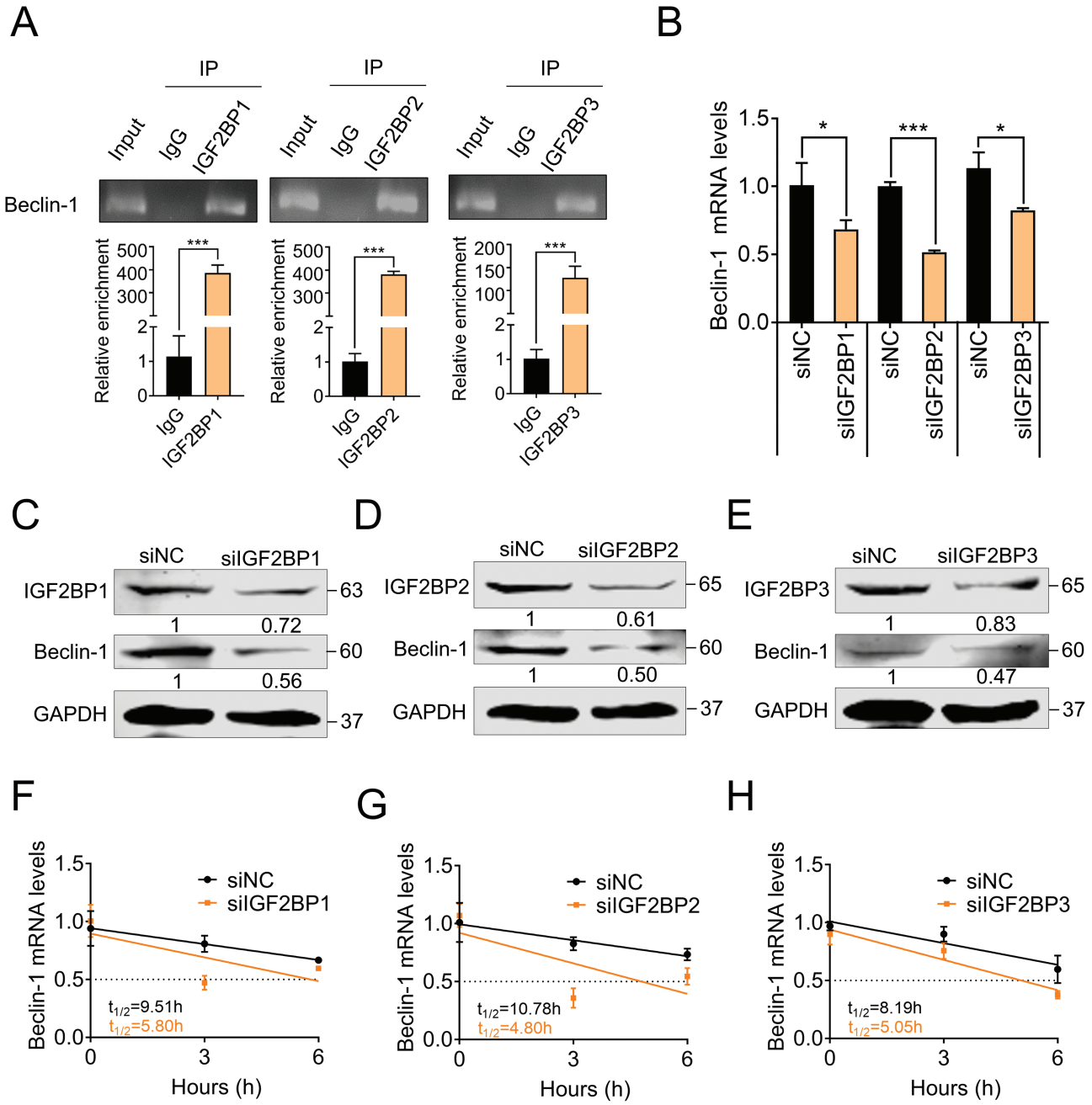

Figure 6. IGF2BP proteins promote the mRNA stability of beclin-1. (A) The RIP-qPCR verified the binding relationship between beclin-1 and IGF2BP1, IGF2BP2, IGF2BP3, respectively. $n = 3$. (B) mRNA expression levels of beclin-1 in BMSCs infected with or without siRNA of IGF2BP1, IGF2BP2, and IGF2BP3 as determined by qRT-PCR. $n = 3$. (C-E) Western blot results show the beclin-1 protein level in siIGF2BP1, siIGF2BP2, and siIGF2BP3. $n = 3$. (F-H) Changes of half-life ($t_{1/2}$) of beclin-1 mRNA in BMSCs with IGF2BP1, IGF2BP2, and IGF2BP3 silencing. $n = 3$. Data are expressed as mean ± SD. $^{*}P < .05$; $^{***}P < .001$.

shown in Fig. 7A, compared to the WT group, osteoclasts in the distal femur of METTL14$^{+/-}$ mice were significantly increased, suggesting stronger bone resorption. Furthermore, after 7 days of RANKL-induction in RAW264.7 cells, the expression levels of osteoclast differentiation-related genes, including TRAP, MMP-9, CTSK, and c-Src were upregulated (Fig. 7B). Meanwhile, the mRNA and protein expression levels of METTL14 were significantly decreased during osteoclastogenesis of RAW264.7 cells (Fig. 7C). Moreover, METTL14 overexpression in RAW264.7 cells led to a significant decrease of TRAP, MMP-9, CTSK, and c-Src (Fig. 7D), while knockdown of METTL14, resulted in a significant upregulation of TRAP, MMP-9, CTSK, and c-Src (Fig. 7E). Taken together, we found that METTL14 plays as an inhibitor role in osteoclast differentiation.

Discussion

In this study, we revealed that METTL14 plays a critical role in the cell fate decision of BMSCs and negatively regulates the osteoporosis process. Our previous study showed that METTL3-based m^{6}A modification favors osteogenic differentiation of BMSCs through the regulation of RUNX2 and pre-miR-320 dependent on m^{6}A modification level.[19] METTL14

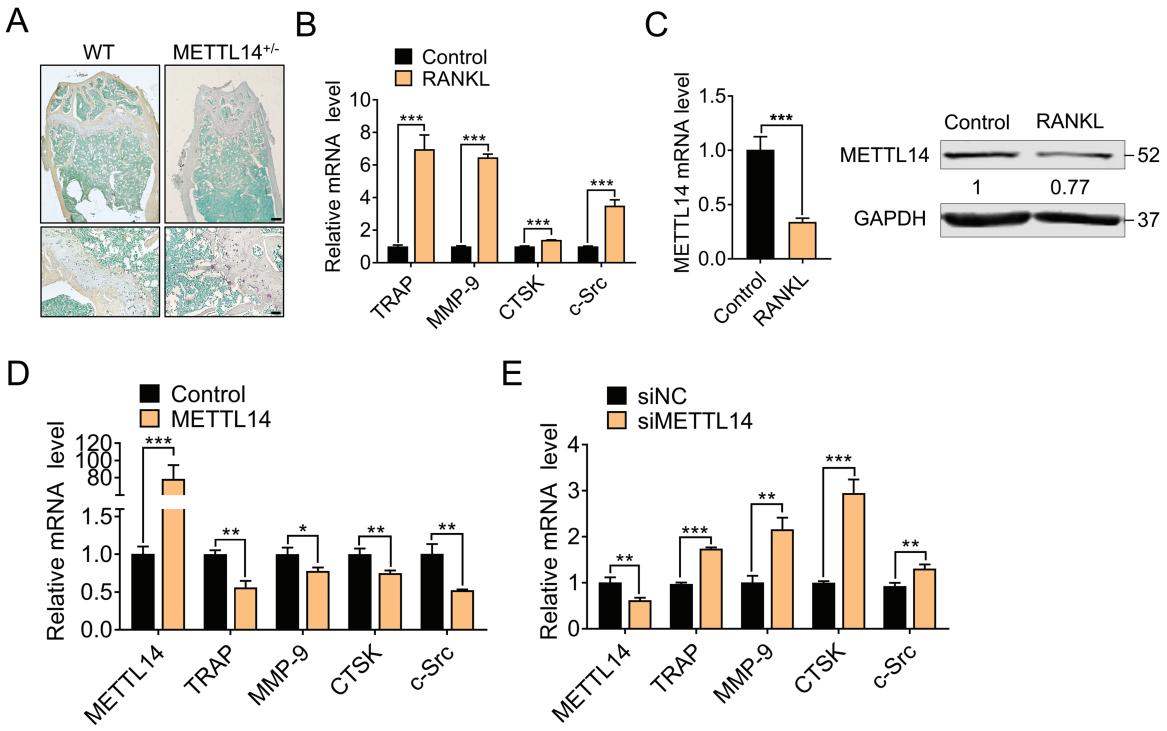

Figure 7. The role of METTL14 in osteoclast differentiation. (A) Representative images of TRAP staining on the distal femur of WT and METTL14$^{+/-}$ mice group. Scale bars show 100 μm in upper line and 20 μm in lower line. $n = 3$. (B) qRT-PCR shows the upregulation of osteoclast marker genes (TRAP, MMP-9, CTSK, c-Src) with RANKL induced in RAW264.7 cells. $n = 3$. (C) METTL14 was downregulated during the osteoclast differentiation of RAW264.7 cells, as shown by qRT-PCR and Western blot analysis. (D) qRT-PCR showed that METTL14 overexpression inhibited the mRNA expression of osteoclast marker genes (TRAP, MMP-9, CTSK, c-Src). (E) METTL14 knockdown increased the expression of the mRNA expression of osteoclast marker genes (TRAP, MMP-9, CTSK, c-Src), as determined by qRT-PCR. $n = 3$. Data are expressed as mean ± SD. *$P < .05$; **$P < .01$; ***$P < .001$.

has also been reported to play an important role in stem cell differentiation.[16,24] Feng et al. have revealed that compared with normal adipose stem cells, the osteogenic differentiation ability of adipose stem cells from osteoporosis rats was significantly downregulated, accompanied by the downregulated expression of METTL14 and Notch1.[6] These studies indicate that osteogenic differentiation ability is positively correlated with METTL14 expression, and Notch1 may be a potential target of METTL14.[6] However, the exact role and the underlying molecular mechanism of METTL14 in the osteoporosis development and osteogenic differentiation remain uncharacterized. Here, we have demonstrated that METTL14 significantly hinders the development of osteoporosis in vivo and promotes osteogenic differentiation of BMSCs in vitro through activating autophagy with the regulation of beclin-1 m^{6}A methylation level. Furthermore, we found that m^{6}A reader proteins IGF2BPs could recognize m^{6}A methylation sites of beclin-1 mRNA and further promote its RNA stabilization and translation.

Here, we found that METTL14 expression was significantly decreased in the bone tissue of patients with osteoporosis and OVX mice compared to normal persons and Sham mice. In our study, normal bone tissues were obtained immediately after surgery for severe fractures in patients younger than 40 years, while the osteoporosis group was derived from patients older than 65 years old, referring to previous methods as reported.[25] It is inevitable that bone resorption will increase and bone formation will decrease with age,[26] which are the pathological factors that affect the process of osteoporosis that we aim to explore in our study. Therefore, we believe that the "age" variable does not affect the judgment of experimental results. Fracture healing process is generally divided into three stages, including hematoma mechanization stage, callus formation stage, and callus remodeling stage.[27] During callus formation, osteoblasts proliferate to form new bone, but this process does not occur until 2 weeks after the fracture.[27] However, since the bone tissue in this study was obtained within 24 hours of the fracture, there is no need to consider the influence of this process on the results.

Autophagy has been reported to play a critical role in the regulation of bone metabolism whose defection accelerates remarkable bone loss and activation alleviates osteoporosis.[28] Accumulating evidence indicates that m^{6}A-related enzymes are involved in autophagy production. Liu et al. demonstrated that METTL3 contributed to increased autophagy by enhancing the expression of autophagy pathway critical genes containing ATG5 and ATG7 in non-small cell lung cancer (NSCLC) cells.[29] Additionally, Li et al. reported that YTHDF1 positively regulated the translation of autophagy-related genes ATG2A and ATG14 upon the combination with m^{6}A modified ATG2A and ATG14 mRNA.[30] Consistently, we demonstrated that compared with wide type mice, METTL14$^{+/-}$ knockdown mice exhibit lower expression level of autophagy-related proteins LC3BII/LC3BI ratio and higher expression level of P62 leading to autophagy defect as well as OVX mice, which further reduces bone formation rate. Of note, autophagy activation also accumulates during osteogenic differentiation of BMSCs following with the increase of METTL14 expression. Therefore, it is possible that the increase of METTL14 expression could reverse autophagic degradation, which was caused by the development of osteoporosis.[28] In vitro, we showed that forced

and downregulated expression of METTL14 significantly promotes and inhibits, respectively, the accumulation of autolysosome and autophagosome.

Autophagosome formation is initiated by the ULK complex, which triggers PI(3)P, a key lipid signaling molecule produced by the phosphatidylinositol 3-kinase (PI3K) complex, downstream production on the phagophore membrane.[31] Beclin-1 is a core component of PI3K complex and plays a central role in autophagy via constituting a molecular platform for the regulation of autophagosome formation and maturation.[31] Previous studies have revealed a strong association between beclin-1 and bone homeostasis which is a regulatory factor for RANKL-induced osteoclast differentiation and chondrocyte differentiation.[32] Our results indicated that beclin-1 exhibits a significant decrease in m^{6}A modification enrichment upon METTL14 knockdown following with the downregulation of both mRNA and protein expression levels. Furthermore, protein expression of beclin-1 was lower in human osteoporosis bone tissues and OVX mice bone tissue compared with normal bone tissues as well as WT mice, respectively. Meanwhile, METTL14 positively regulated mRNA and protein stabilization of beclin-1. Therefore, we hypothesized that METTL14 regulates beclin-1 expression depending on m^{6}A modification to activate autophagy signaling pathway. Furthermore, 3-MA, an autophagy inhibitor, has been reported to enhance the adipogenic differentiation ability of young BMSCs as well as decrease their osteogenic differentiation and proliferation ability, leading to their relative aging state.[33] As expected, 3-MA decreased the osteogenic differentiation ability promoted by METTL14 overexpression, while forced expression of beclin-1 recused osteogenic differentiation defects caused by METTL14 silence.

M^{6}A readers have been reported to be involved in the fate of mRNA by regulating pre-mRNA splicing, facilitating translation, or controlling mRNA decay and protein stability. M^{6}A readers IGF2BP proteins were proven to enhance mRNA stability and translation via recognizing RNA m^{6}A.[22] Li et al. have shown that IGF2BP2 prevents sex-determining region Y-box 2 (SOX2) mRNA degradation via recognizing the coding sequence (CDS) regions in colorectal cancer cells.[34] Thus, our data presented that IGF2BPs are directly bound to beclin-1 mRNA in an m^{6}A-dependent manner. Additionally, knockdown of IGF2BP1/2/3 markedly inhibits the protein level of beclin-1 by controlling the beclin-1 mRNA half-life, indicating that IGF2BP proteins regulate beclin-1 transcript stability by identifying METTL14-mediated m^{6}A modification sites and further promotes its translation.

The important mechanism by which m^{6}A-dependent regulation genes is to promote protein stability through the reader proteins YTHDF1, YTHDF2, and YTHDC1, thus promoting translation efficiency.[35,36] Notably, METTL14 also could positively regulate beclin-1 protein stabilization in BMSCs remaining possible that there could be indirect effects caused by other m^{6}A readers. However, the shortcoming of this study is that we did not identify specific regulatory reading proteins, which we will explore in the future research. Notwithstanding its limitation, this study does suggest that METTL14 is important for the treatment of osteoporosis by targeting beclin-1 to promote its translation and activate autophagy.

Conclusion

In conclusion, we provided compelling in vitro and in vivo evidence demonstrating that METTL14, an m^{6}A methyltransferase, plays a critical role in the maintenance of osteogenic differentiation ability of BMSCs and in the obstruction of the osteoporosis progression, through enhancing m^{6}A modification levels in mRNA transcripts of its critical target gene beclin-1, thereby triggering autophagy signaling pathway. Additionally, we revealed that the regulatory network between m^{6}A writer METTL14, m^{6}A readers IGF2BPs, and target gene beclin-1 pointed out an innovative regulatory mechanism based on m^{6}A modification. Furthermore, METTL14 could negatively regulate osteoclast differentiation of macrophages and further inhibit bone resorption. Given the functional importance of METTL14 in bone formation, METTL14 might be a new marker for osteoporosis development, and targeting METTL14-IGF2BPs-beclin-1 signaling axis by selective promoters may represent a promising therapeutic strategy to treat osteoporosis.

Funding

This work was supported by grants from the National Natural Science Fund of China (81972117), Natural Science Foundation of Heilongjiang Province of China for excellent youth (JJ2020JQ0004), The First Affiliated Hospital of Harbin Medical University Excellent Young Talents Funding (HYD2020JQ0013), Natural Science Foundation of Heilongjiang Province of China for outstanding youth (YQ2020H019), and Chinese Academy of Medical Sciences (CAMS) Innovation Fund for Medical Sciences (CIFMS, 2020-I2M-5-003), and Harbin Medical University (HMU) Marshal Initiative Funding (HMUMIF-21009).

Conflict of Interest

The authors declared no potential conflicts of interest.

Author Contributions

Y.Y. and L.Y. designed the study. Y.Y., M.H., H.L., X.H., Y.L., A.W., Z.R., X.L., G.Y., W.W., Y.W., G.L., and T.W. performed research; Y.Y., M.H., H.L., X.H., J.P., Z.S., and W.D. analyzed data; Y.Y., M.H. H.L., and X.H. wrote the manuscript. All authors revised the manuscript and approved the final version.

Ethics Approval and Consent to Participate

Written informed consent was obtained from all participants in accordance with the Declaration of Helsinki. All the collection of specimens and animal handling in this study was reviewed and approved by the Medical Ethics Committee of the First Affiliated Hospital of Harbin Medical University.

Data Availability

The data that support the findings of this study are available from the corresponding author upon reasonable request.

Supplementary Material

Supplementary material is available at *Stem Cells Translational Medicine* online.

References

1. Levine B, Kroemer G. Autophagy in the pathogenesis of disease. *Cell*. 2008;132(1):27-42. https://doi.org/10.1016/j.cell.2007.12.018
2. Chang C, Jensen LE, Hurley JH. Autophagosome biogenesis comes out of the black box. *Nat Cell Biol*. 2021;23(5):450-456. https://doi.org/10.1038/s41556-021-00669-y
3. Li H, Li D, Ma Z, et al. Defective autophagy in osteoblasts induces endoplasmic reticulum stress and causes remarkable bone loss. *Autophagy*. 2018;14(10):1726-1741. https://doi.org/10.1080/15548627.2018.1483807
4. Shen GS, Zhou HB, Zhang H, et al. The GDF11-FTO-PPARgamma axis controls the shift of osteoporotic MSC fate to adipocyte and inhibits bone formation during osteoporosis. *Biochim Biophys Acta Mol Basis Dis*. 2018;1864(12):3644-3654. https://doi.org/10.1016/j.bbadis.2018.09.015
5. Qi M, Zhang L, Ma Y, et al. Autophagy maintains the function of bone marrow mesenchymal stem cells to prevent estrogen deficiency-induced osteoporosis. *Theranostics*. 2017;7(18):4498-4516. https://doi.org/10.7150/thno.17949
6. Feng MG, Yang SL, Luo DW, et al. Osteogenic capacity and Mettl14 and notch1 expression of adipose-derived stem cells from osteoporotic rats. *Sichuan Da Xue Xue Bao Yi Xue Ban*. 2021;52(3):423-429. https://doi.org/10.12182/20210560502
7. Onal M, Piemontese M, Xiong J, et al. Suppression of autophagy in osteocytes mimics skeletal aging. *J Biol Chem*. 2013;288(24):17432-17440. https://doi.org/10.1074/jbc.M112.444190
8. King KE, Losier TT, Russell RC. Regulation of autophagy enzymes by nutrient signaling. *Trends Biochem Sci*. 2021;46(8):687-700. https://doi.org/10.1016/j.tibs.2021.01.006
9. Kroemer G, Mariño G, Levine B. Autophagy and the integrated stress response. *Mol Cell*. 2010;40(2):280-293. https://doi.org/10.1016/j.molcel.2010.09.023
10. Wang P, Doxtader KA, Nam Y. Structural basis for cooperative function of Mettl3 and Mettl14 methyltransferases. *Mol Cell*. 2016;63(2):306-317. https://doi.org/10.1016/j.molcel.2016.05.041
11. Ping X-L, Sun B-F, Wang L, et al. Mammalian WTAP is a regulatory subunit of the RNA N6-methyladenosine methyltransferase. *Cell Res*. 2014;24(2):177-189. https://doi.org/10.1038/cr.2014.3
12. Jia G, Fu Y, Zhao X, et al. *N*6-methyladenosine in nuclear RNA is a major substrate of the obesity-associated FTO. *Nat Chem Biol*. 2011;7(12):885-887. https://doi.org/10.1038/nchembio.687
13. Zheng G, Dahl JA, Niu Y, et al. ALKBH5 is a mammalian RNA demethylase that impacts RNA metabolism and mouse fertility. *Mol Cell*. 2013;49(1):18-29. https://doi.org/10.1016/j.molcel.2012.10.015
14. Yuan Y, Yan G, He M, et al. ALKBH5 suppresses tumor progression via an m^{6}A-dependent epigenetic silencing of pre-miR-181b-1/YAP signaling axis in osteosarcoma. *Cell Death Dis*. 2021;12(1):60. https://doi.org/10.1038/s41419-020-03315-x
15. Wang L, Hui H, Agrawal K, et al. m^{6}A RNA methyltransferases METTL3/14 regulate immune responses to anti-PD-1 therapy. *EMBO J*. 2020;39(20):e104514. https://doi.org/10.15252/embj.2020104514
16. Weng H, Huang H, Wu H, et al. METTL14 inhibits hematopoietic stem/progenitor differentiation and promotes leukemogenesis via mRNA m^{6}A modification. *Cell Stem Cell*. 2018;22(2):191-205.e9. https://doi.org/10.1016/j.stem.2017.11.016
17. Mo XB, Zhang YH, Lei SF. Genome-wide identification of m^{6}A-associated SNPs as potential functional variants for bone mineral density. *Osteoporos Int*. 2018;29(9):2029-2039. https://doi.org/10.1007/s00198-018-4573-y
18. He Y, Wang W, Xu X, et al. Mettl3 inhibits the apoptosis and autophagy of chondrocytes in inflammation through mediating Bcl2 stability *via* Ythdf1-mediated m^{6}A modification. *Bone*. 2022;154:116182. https://doi.org/10.1016/j.bone.2021.116182
19. Yan G, Yuan Y, He M, et al. m^{6}A methylation of precursor-miR-320/RUNX2 controls osteogenic potential of bone marrow-derived mesenchymal stem cells. *Mol Ther Nucleic Acids*. 2020;19:421-436. https://doi.org/10.1016/j.omtn.2019.12.001
20. Lin Z, Hsu PJ, Xing X, et al. Mettl3-/Mettl14-mediated mRNA *N*^{6}-methyladenosine modulates murine spermatogenesis. *Cell Res*. 2017;27(10):1216-1230. https://doi.org/10.1038/cr.2017.117
21. Jing H, Liao L, An Y, et al. Suppression of EZH2 prevents the shift of osteoporotic MSC fate to adipocyte and enhances bone formation during osteoporosis. *Mol Ther*. 2016;24(2):217-229. https://doi.org/10.1038/mt.2015.152
22. Huang H, Weng H, Sun W, et al. Recognition of RNA *N*^{6}-methyladenosine by IGF2BP proteins enhances mRNA stability and translation. *Nat Cell Biol*. 2018;20(3):285-295. https://doi.org/10.1038/s41556-018-0045-z
23. Ma Y, Ran D, Zhao H, et al. Cadmium exposure triggers osteoporosis in duck via P2X7/PI3K/AKT-mediated osteoblast and osteoclast differentiation. *Sci Total Environ*. 2021;750:141638. https://doi.org/10.1016/j.scitotenv.2020.141638
24. Wang Y, Li Y, Yue M, et al. *N*^{6}-methyladenosine RNA modification regulates embryonic neural stem cell self-renewal through histone modifications. *Nat Neurosci*. 2018;21(2):195-206. https://doi.org/10.1038/s41593-017-0057-1
25. Wang H, Hu Z, Wu J, et al. Sirt1 promotes osteogenic differentiation and increases alveolar bone mass via Bmi1 activation in mice. *J Bone Miner Res*. 2019;34(6):1169-1181. https://doi.org/10.1002/jbmr.3677
26. Lewis JW, Edwards JR, Naylor AJ, et al. Adiponectin signalling in bone homeostasis, with age and in disease. *Bone Res*. 2021;9(1):1. https://doi.org/10.1038/s41413-020-00122-0
27. Einhorn TA, Gerstenfeld LC. Fracture healing: mechanisms and interventions. *Nat Rev Rheumatol*. 2015;11(1):45-54. https://doi.org/10.1038/nrrheum.2014.164
28. Liu ZZ, Hong CG, Hu WB, et al. Autophagy receptor OPTN (optineurin) regulates mesenchymal stem cell fate and bone-fat balance during aging by clearing FABP3. *Autophagy*. 2021;17(10):2766-2782. https://doi.org/10.1080/15548627.2020.1839286.
29. Liu S, Li Q, Li G, et al. The mechanism of m^{6}A methyltransferase METTL3-mediated autophagy in reversing gefitinib resistance in NSCLC cells by β-elemene. *Cell Death Dis*. 2020;11(11):969.
30. Li Q, Ni Y, Zhang L, et al. HIF-1α-induced expression of m6A reader YTHDF1 drives hypoxia-induced autophagy and malignancy of hepatocellular carcinoma by promoting ATG2A and ATG14 translation. *Signal Transduct Target Ther*. 2021;6(1):76. https://doi.org/10.1038/s41392-020-00453-8
31. Hill SM, Wrobel L, Rubinsztein DC. Post-translational modifications of Beclin 1 provide multiple strategies for autophagy regulation. *Cell Death Differ*. 2019;26(4):617-629. https://doi.org/10.1038/s41418-018-0254-9
32. Arai A, Kim S, Goldshteyn V, et al. Beclin1 modulates bone homeostasis by regulating osteoclast and chondrocyte differentiation. *J Bone Miner Res*. 2019;34(9):1753-1766. https://doi.org/10.1002/jbmr.3756
33. Ma Y, Qi M, An Y, et al. Autophagy controls mesenchymal stem cell properties and senescence during bone aging. *Aging Cell*. 2018;17(1):e12709. https://doi.org/10.1111/acel.12709
34. Li T, Hu PS, Zuo Z, et al. METTL3 facilitates tumor progression via an m^{6}A-IGF2BP2-dependent mechanism in colorectal carcinoma. *Mol Cancer*. 2019;18(1):112. https://doi.org/10.1186/s12943-019-1038-7
35. Wang X, Zhao BS, Roundtree IA, et al. *N*^{6}-methyladenosine modulates messenger RNA translation efficiency. *Cell*. 2015;161(6):1388-1399. https://doi.org/10.1016/j.cell.2015.05.014
36. Ru W, Zhang X, Yue B, et al. Insight into m^{6}A methylation from occurrence to functions. *Open Biol*. 2020;10(9):200091. https://doi.org/10.1098/rsob.200091